

Production of π^0 and η^0 at 11° in pp Collisions at $\sqrt{s} = 63$ GeV

The Axial Field Spectrometer Collaboration

T. Akesson⁴, M.G. Albrow⁶, S. Almedhed⁴, R. Batley², O. Benary⁷, H. Bøggild³, O. Botner², H. Brody⁵,
V. Burkert², R. Carosi⁸, W. Cleland⁹, D. Cockerill⁶, S. Dagan⁷, E. Dahl-Jensen³, I. Dahl-Jensen³,
G. Damgaard³, A. Di Ciaccio¹, W.M. Evans⁶, C.W. Fabjan², P. Frandsen², S. Frankel⁵, W. Frati⁵, H. Gordon¹,
U. Goerlach², A. Hallgren², K.H. Hansen³, M. Harris², B. Heck², H.J. Hilke², J.E. Hooper³, G. Jarlskog⁴,
P. Jeffreys⁶, T. Jensen², G. Kessler², T. Killian¹, R. Kroeger⁹, J. v. d. Lans², D. Lissauer⁷, B. Lörstad⁴,
H. Lubatti^{2**}, T. Ludlam¹, I. Mannelli², A. Markou², N.A. McCubbin⁶, F. Meyer², U. Mjörnmark⁴, R. Møller³,
W. Molzon⁵, A. Nappi⁸, B.S. Nielsen², A. Nilsson⁴, L.H. Olsen², Y. Oren⁷, G. Pierazzini⁸, L. Rosselet²,
E. Rosso², R.H. Schindler^{2*}, B. Schistad³, I. Stumer¹, M. Sullivan⁹, J. Thompson⁹, E. Vella⁵,
W.J. Willis², M. Winik¹, W. Witzeling² and C. Woody¹

Received 7 February 1983

Abstract. The inclusive π^0 production cross-section and the η/π^0 ratio have been measured in pp collisions at $\sqrt{s} = 63$ GeV at the CERN Intersecting Storage Rings in the rapidity range $2.00 < y < 2.75$. The π^0 cross-section exhibits a strong y -dependence and falls more steeply as a function of p_T , compared with the cross-section measured at $y \sim 0$. We find a value of 0.46 ± 0.07 for the η/π^0 ratio with no significant p_T dependence over the range $2.0 < p_T < 4.0$ GeV/c.

1. Introduction

Measurements of π^0 production at small centre-of-mass angles [1, 2] have shown that the cross-section changes rapidly as a function of p_T and y , decreasing sharply as one approaches the forward direction. Previous measurements in this region at CERN Intersecting Storage Rings (ISR) energies [1] were not

able to resolve the two photons from the decay and could not distinguish between π^0 's, η 's, and single photons. The measurements here were carried out using a fine-grained uranium-scintillator sandwich calorimeter with good energy and position resolution, capable of resolving π^0 's with energies up to ~ 25 GeV ($p_T \sim 4.5$ GeV/c). We have measured the p_T and y dependence of the π^0 cross-section at $\sqrt{s} = 63$ GeV in the region $1.0 < p_T < 4.0$ GeV/c, $2.00 < y < 2.75$, and the ratio η/π^0 as a function of p_T in the range $2.0 < p_T < 4.0$ GeV/c. The results are compared with measurements at the same energy at $y \sim 0$ [3, 4] and with measurements in the same rapidity range at lower centre-of-mass energies [1, 2, 5].

2. Apparatus

The calorimeter, shown in Fig. 1, was a part of the Axial Field Spectrometer (AFS) at the CERN ISR. A detailed description of the AFS and the small-angle calorimeter can be found in Refs. 6 and 7 respectively. The calorimeter was located at a distance of 1.76 m from the intersection region. It was centred at an angle of 11° with respect to one outgoing beam and subtended a solid angle of 25 msr. At this position, good energy and spatial resolution are required to resolve the two photons from the decay of high-energy π^0 's. This resolution was achieved by the use of uranium as a showering material, result-

1 Brookhaven National Laboratory, Upton, NY, USA

2 CERN, Geneva, Switzerland

3 Niels Bohr Institute, Copenhagen, Denmark

4 University of Lund, Sweden

5 University of Pennsylvania, Philadelphia, USA

6 Rutherford Appleton Laboratory, Didcot, UK

7 University of Tel-Aviv, Israel

8 INFN and Istituto di Fisica dell'Università, Pisa, Italy

9 University of Pittsburgh, Pittsburgh, PA, USA

* Present address: California Institute of Technology, Pasadena, CA 91125, USA

** Visitor from the University of Washington, Seattle, WA, USA

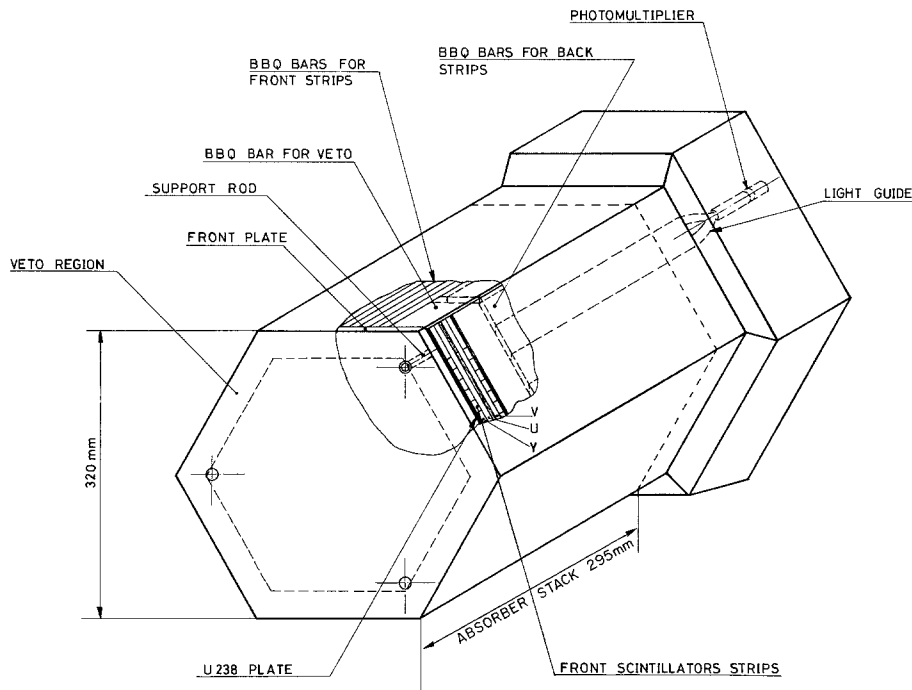


Fig. 1. Hexagon calorimeter

ing in a compact design, and by the use of narrow scintillator strips. The readout consisted of three views (Y, U, V) arranged in a hexagonal geometry. The views were composed of layers of 2.5 mm thick scintillator strips interleaved between 1.6 mm thick uranium plates. The scintillators were arranged with two views per gap, rotated by an angle of 120° with respect to each other. The calorimeter was divided into a front section, 6.5 radiation lengths (0.47 interaction lengths) in depth, and a back section, 13.0 radiation lengths (0.93 interaction lengths). The front section consisted of a fiducial region of twenty-four 1 cm wide strips for each view, surrounded by a 3.5 cm wide veto region. The back section consisted of ten 3 cm wide strips for each view. The strips were read out on one end around the perimeter of the hexagon using wavelength shifter (BBQ) bars coupled to photomultiplier tubes (PMs). The dynode signals from the PMs were used for triggering, and the anode outputs were recorded by ADCs.

The accuracy in determining the position of single isolated showers was measured in a test beam of electrons and found to be $\sigma_x \sim 2.3$ mm. The minimum shower separation for resolving two showers was ~ 2 cm. An energy resolution of $\sigma(E)/E \approx 0.11/\sqrt{E}$ was obtained for electrons, consistent with the resolution computed using the EGS Monte Carlo program [8].

The division into front and back sections provided information on the longitudinal development of the showers and was used in discriminating against hadrons. The e/π rejection was measured in

a test beam of 7 GeV electrons and π^- 's, and an upper limit of 1% (limited by the ability to identify electrons in the beam) was obtained for the probability for a hadron to be misidentified as an electron with an energy $\geq 80\%$ of the beam energy. This rejection was achieved with an electron efficiency of 96%.

The relative gains for the phototubes were determined in the test beam using minimum-ionizing particles in each strip. The calibration was maintained using the uranium radioactivity as a calibration source.

3. Trigger

The trigger demanded a signal indicating that a minimum energy had been deposited in the calorimeter in coincidence with a "minimum bias" trigger from the AFS, which required an inelastic event to have occurred in the interaction region. The calorimeter signal was formed by adding the dynode outputs of the PMs from the front and back sections for the $Y, U,$ and V views separately. The calorimeter was oriented with the scintillator strips in the U view parallel to the direction defining p_T in the laboratory, and were read out at the end farthest away from the beam, as shown in Fig. 2. This resulted in producing more observed light for a given energy deposition near the phototube end of the strips, compared with the opposite end, because of the light attenuation in the scintillator. The light output varied roughly as the inverse of the distance from the

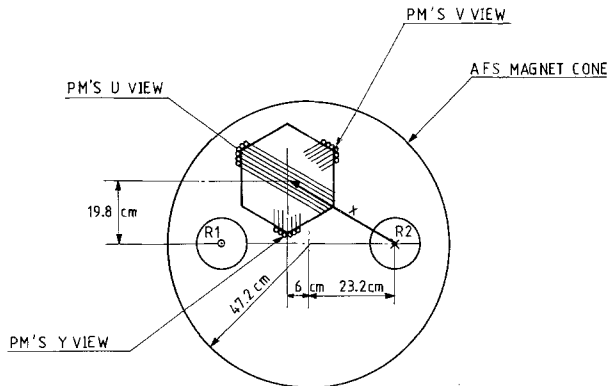


Fig. 2. Location of the calorimeter in the transverse plane as viewed from the intersection. The magnet cone is shown at the longitudinal position of the calorimeter. R1(R2) is incoming (outgoing) proton beam

readout end, and, since $p_T = E \sin \theta$ increases linearly with x , triggering on a threshold for the observed pulse height resulted in a trigger threshold of approximately constant p_T over the region covered by the calorimeter.

A minimum energy deposition was required in the U view, which defined the p_T of the trigger, in addition to corroborating energy in the other two views. In these views the variation in pulse height was not related to p_T in a simple way, and the thresholds were set a factor of 3 lower than in the U view.

The minimum bias trigger utilized two sets of scintillation counters. The first, called the “beam-beam” counters, were a set of small-angle counters located around the two outgoing beams in the forward direction and covered an angular range $2^\circ < \theta < 6^\circ$. The second set, the “barrel hodoscope” consisted of 44 scintillators, 54 cm in length, arranged azimuthally around the central intersection region at a radius of 18 cm. The minimum bias trigger required either a coincidence of the beam-beam counters from each outgoing beam or a signal from the barrel hodoscope. The combination of the beam-beam and barrel hodoscope counters was sensitive to $\sim 80\%$ of the total pp inelastic cross-section ($\geq 95\%$ of the non-diffractive cross-section). The final trigger required a coincidence between the calorimeter signal and the minimum bias trigger.

A total of 623,000 events were collected with an average luminosity of $1.5 \times 10^{31} \text{ cm}^{-2} \text{ s}^{-1}$. The trigger system of the AFS allowed the calorimeter trigger to run in a dedicated mode, or in parallel with other triggers in the system. The low- p_T data ($p_T < 3 \text{ GeV}/c$) were taken during dedicated runs corresponding to an integrated luminosity of $2.33 \times 10^{35} \text{ cm}^{-2}$. The high- p_T data were taken in paral-

lel with other triggers and correspond to an integrated luminosity of $6.83 \times 10^{36} \text{ cm}^{-2}$,

4. Data Analysis

The raw data were corrected for pedestals and slopes of the ADC's and a small non-linearity in the response of the phototubes at high energies. The non-linearity was measured for each PM using an external light-source coupled to the phototubes by a system of optical fibers. The non-linearity correction increased the π^0 energy by less than 1% at 20 GeV. A cut of 25 MeV was applied to the corrected pulse heights to suppress the uranium noise before being used in the analysis. This removed 99.4% of the noise from the front strips and 95.3% from the back.

The data were processed with a pattern recognition program which reconstructed the shower energies and positions using the calorimeter information. The program searched for peaks in each view separately, and required agreement in position and energy between the views to define a shower. The energies of peaks which partially overlapped were corrected for the amount of shared energy using the transverse shape of electron showers measured in a test beam. The shower energies were determined from a fit using the peak pulse-heights and positions from each view, and included the corrections for light attenuation in the strips.

The conversion from ADC pulse height to energy was determined by comparing π^0 events in the real data with those generated with a Monte Carlo program. The Monte Carlo incorporated the known geometry of the detector, the effect of light attenuation in the scintillator strips, and the uranium noise. It was used to generate π^0 's with a production spectrum and vertex distribution which simulated actual ISR conditions. The shower development in the calorimeter was simulated with the EGS program. A careful study was carried out to ensure that the showers generated by EGS reproduced the characteristics of real showers measured in the test beam and at the ISR. Good agreement was found between all features of the real and Monte Carlo generated showers, except for the transverse energy spread. This was attributed to the following reasons: *i*) the Monte Carlo program did not adequately describe the detailed geometry of the calorimeter in terms of gaps between the strips and plates; *ii*) a small amount of optical cross-talk between the scintillators, *BBQ* bars, and light-guides; and *iii*) the possibility that EGS did not describe exactly the tails of the energy deposition far away from the central part of the shower. Since the π^0 reconstruction efficiency at high p_T was affected by the lateral shape, a correc-

tion was made to the showers generated by EGS to redistribute the energy in the front section according to the transverse shape measured for real showers. This correction shifted the average value of the radius for a single shower from 6.3 to 8.3 mm.

The Monte Carlo program produced simulated pulse heights for each phototube which were used as input to the standard pattern recognition program. The conversion factor from simulated pulse heights to GeV was determined by generating single-photon showers with a known energy and requiring that the reconstructed energy be, on the average, the same as that of the original photon. When this factor was applied to the π^0 events generated with the same program, the correct energy for the π^0 was obtained, but the average value of the π^0 mass was 131.1 MeV. This shift from the true value for the π^0 mass was attributed to a slight distortion in the energy sharing and relative shower separation as calculated by the reconstruction program for showers which were close together. The conversion factor from pulse height to GeV for the real data was adjusted such that the reconstructed π^0 mass in the real data gave the same average value. The uncertainty in the absolute energy scale introduced by this method was estimated to be $\pm 3\%$.

The raw data were selected requiring at least one $\gamma\gamma$ mass combination above a certain p_T . The p_T cut was chosen to be well above the trigger threshold to ensure that the selected events were not affected by any trigger inefficiency. This resulted in retaining $\sim 25\%$ of the raw events for the final analysis. Each shower in the selected events was then subjected to the following criteria:

- i) to be within a fiducial region at least 1 cm from the veto region;
- ii) 400 MeV minimum energy deposition in the whole calorimeter;
- iii) 200 MeV minimum energy deposition in the front section;
- iv) $E_{\text{front}}/E_{\text{total}} > 0.2$.

The $\gamma\gamma$ effective mass was computed for all photon pairs passing these cuts. Figure 3 shows the mass distribution for $\gamma\gamma$ pairs with $p_T > 3.0$ GeV/c. The width of the π^0 peak is $\sigma \sim 11\%$, in agreement with the value obtained with the Monte Carlo program. The width of the η is $\sigma \sim 8\%$ and also agrees with the Monte Carlo calculation.

The background under the π^0 and η peaks was mainly due to combinatorial background from additional photons in the event and to hadronic showers not eliminated by the cuts. There was also the background from non-beam-beam interactions, such as beam-gas events, and beam-halo events from par-

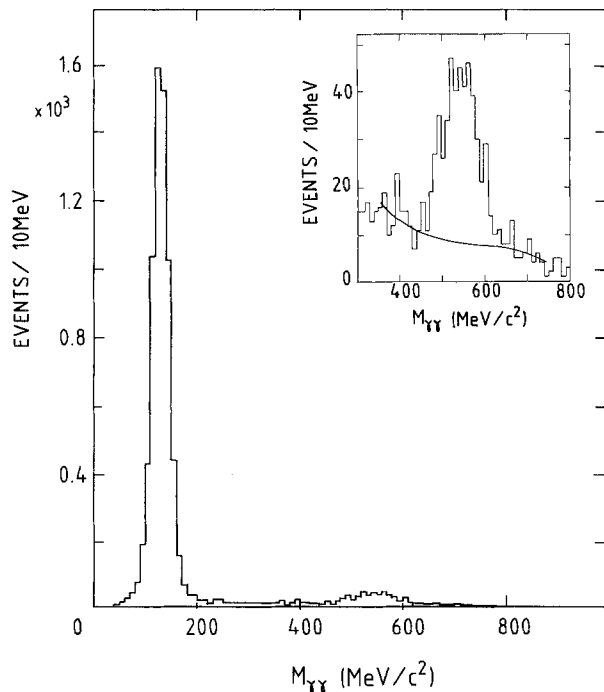


Fig. 3. Gamma-gamma invariant mass for photons passing cuts and p_T of the $\gamma\gamma$ pair greater than 3.0 GeV/c. Insert shows η mass region enlarged with fitted background curve

ticles outside the beam which interacted with material in the ISR. These events were a possible source of background since no vertex requirement was made in the analysis. The events occurring outside of the interaction region produced particles which entered the calorimeter either from behind or from the front at an oblique angle. Hadronic showers of this type were largely eliminated by the longitudinal shower development cut. The backgrounds from secondary interactions in the vacuum chamber and from cosmic rays were negligible.

The $\gamma\gamma$ mass distributions were fitted in the region of the π^0 and η to a Gaussian peak plus a polynomial background. The background was determined from the fit and subtracted to give the true π^0 and η signals. The background varied from 27% at $p_T=1$ GeV/c to 8% at $p_T=4$ GeV/c for the π^0 , and 50% at $p_T=2$ GeV/c to 20% at $p_T=4.0$ GeV/c for the η .

5. Corrections for Efficiency and Acceptance

The geometrical acceptance and reconstruction efficiency were calculated using the Monte Carlo program. Neutral pions and η 's were generated with a spectrum given by $A(p_T^2 + m^2)^N(1 - x_R)^M$ where $x_R = 2p/\sqrt{s}$, using the parameters for $\theta_{\text{cm}} = 8^\circ$ given in [1] and listed in Table 1. The parameters were varied over limits consistent with the fits to this form

Table 1. Fits to the form $A(p_T^2 + m^2)^N(1 - x_R)^M$; $x_R = 2p/\sqrt{s}$

	This experiment	$\sqrt{s} = 53$ $\theta_{cm} \sim 8^\circ$ Ref. 1	$\sqrt{s} = 53$ $\theta_{cm} \sim 17^\circ$ Ref. 1	$\sqrt{s} = 13.8, 19.4$ GeV $15^\circ < \theta_{cm} < 115^\circ$ Ref. 2
A ($\text{cm}^2 \text{GeV}^{-2}$)	$1.21 \pm 0.06 \times 10^{-26}$	3.69×10^{-26}	1.80×10^{-26}	$1.22 \pm 0.15 \times 10^{-26}$
m (GeV/c^2)	1.03 ± 0.01	1.111	1.121	0.90 ± 0.02
N	-4.32 ± 0.08	-5.04	-4.64	-4.90 ± 0.06
M	6.39 ± 0.22	4.02	2.94	4.42 ± 0.05
χ^2/DOF	66/65	188/87	153/131	306/142

from our own measurements in order to determine the sensitivity of the acceptance and efficiency calculations to the parametrization used in the generation. The reconstruction efficiency was computed for both the π^0 and η by simulating events with the Monte Carlo program and analysing these events with the same pattern recognition program and cuts as those used for the real data.

Figure 4a shows the combined geometrical acceptance and reconstruction efficiency for π^0 's in three rapidity intervals. The variation with y is mainly due to the different solid-angle coverage of the calorimeter at different θ_{cm} . Figure 4b shows the combined acceptance and efficiency for the η relative to the π^0 averaged over the rapidity range $2.00 < y < 2.75$. The bands indicate the statistical and systematic errors from the Monte Carlo calculation of the efficiencies, and the systematic error on the acceptance due to the uncertainty in the production spectrum.

The corrections for energy resolution and leakage of energy out of the back of the calorimeter were taken into account by the Monte Carlo program. The back leakage, calculated by EGS, varied from 2% for 4 GeV showers to 4% for 20 GeV showers.

6. π^0 Cross-Sections

The absolute normalization for the π^0 cross-section was determined using the luminosity measured with the beam-beam counters. The constant for converting from the observed rates in these counters to luminosity was measured periodically throughout the experiment during special ISR runs. The error in the normalization introduced by the uncertainty in the luminosity measurement was 6%. The cross-sections were also corrected by a factor of 1.25 for the fraction of the total inelastic pp cross-section which did not satisfy the minimum bias trigger. This correction assumes that the events which did not satisfy the trigger had the same probability for producing a π^0 in the calorimeter as those which did satisfy the trigger.

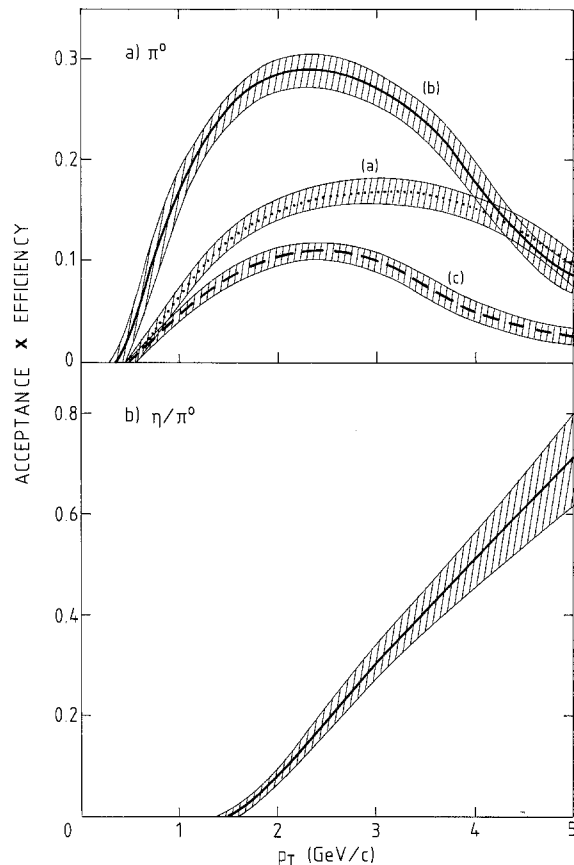


Fig. 4a. Combined geometrical acceptance and reconstruction efficiency for π^0 's versus p_T . Curve (a) is for $2.00 < y < 2.25$, curve (b) $2.25 < y < 2.50$, and curve (c) $2.50 < y < 2.75$. Normalization is to the interval $\Delta y = 0.25$, $\Delta \phi = 1.7$ rad. **b** Combined geometrical acceptance and reconstruction efficiency for η 's relative to π^0 's versus p_T for $2.00 < y < 2.75$. The bands indicate the statistical and systematic errors

The observed number of π^0 's was determined from the fits to the signal plus background as a function of p_T in the mass range $90 < m_{\gamma\gamma} < 170$ MeV. The number of π^0 's was corrected for geometrical acceptance and reconstruction efficiency and converted to an invariant cross-section using the measured values for the luminosity. The data for each trigger threshold were normalized independently and used

to compute a weighted average for the cross-section in each $y-p_T$ bin. The combining together of runs taken at different thresholds leads to an additional systematic error of 15% on the final cross-section. Figure 5 and Table 2 give the invariant cross-section as a function of p_T in three y intervals. The errors given are the combined statistical and systematic errors. The effects of the systematic errors on the final cross-section are listed in Table 3.

The cross-section decreases rapidly with increasing y over the rapidity range covered. The result of a fit of our data to the form $A(p_T^2+m^2)^N(1-x_R)^M$ as suggested by radial scaling [9] is listed in Table 1 along with the values given in [1] for $\theta_{\text{cm}} \sim 8^\circ$ and $\theta_{\text{cm}} \sim 17^\circ$ at $\sqrt{s}=53$ GeV, and from Ref. 2 for $15^\circ < \theta_{\text{cm}} < 115^\circ$ for \sqrt{s} in the range 14–24 GeV. The fit to our data gives a steeper x_R (and hence y) dependence and a less steep p_T dependence than the other results. It should be noted, however, that the parameters N and M are highly correlated, reflecting the fact that it is difficult to determine simultaneously the p_T and x_R dependence of the cross-section with data over a limited range of rapidity at fixed \sqrt{s} . Part of the difference between the fitted parameters may also be attributed to the fact that the π^0 's in [1] were unresolved, and hence more susceptible to background, whilst [2], although for resolved π^0 's, was at a significantly lower \sqrt{s} . Figure 5 also shows data at 90° for $p_T > 3.0$ GeV/c for the

same \sqrt{s} from [3] (Kourkoumelis et al.). The cross-section at large rapidity is smaller and decreases more rapidly as a function of p_T than the data at $y \sim 0$. This effect was also observed at lower energies [1, 2].

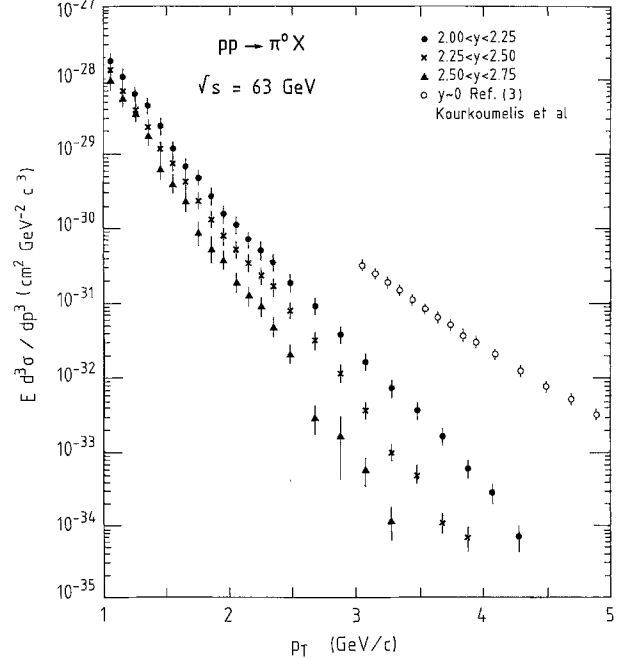


Fig. 5. Invariant π^0 cross-section. Closed circles are for $2.00 < y < 2.25$, crosses $2.25 < y < 2.50$, and triangles $2.50 < y < 2.75$. Errors are statistical and systematic. Open circles are data at $y \sim 0$ from Ref. 3 (Kourkoumelis et al.)

Table 2. Invariant cross-section $pp \rightarrow \pi^0 X$, $\sqrt{s}=63$ GeV

p_T range (GeV/c)	$\langle p_T \rangle$ (GeV/c)	$E(d^3\sigma/dp^3)(\text{cm}^2 \text{GeV}^{-2} \text{c}^3)$		
		$2.00 < y < 2.25$	$2.25 < y < 2.50$	$2.50 < y < 2.75$
1.0–1.1	1.05	$1.81 \pm 0.44 \times 10^{-28}$	$1.38 \pm 0.34 \times 10^{-28}$	$9.93 \pm 2.51 \times 10^{-29}$
1.1–1.2	1.15	$1.09 \pm 0.27 \times 10^{-28}$	$6.59 \pm 1.62 \times 10^{-29}$	$5.74 \pm 1.48 \times 10^{-29}$
1.2–1.3	1.25	$6.31 \pm 1.58 \times 10^{-29}$	$3.47 \pm 0.86 \times 10^{-29}$	$3.74 \pm 0.99 \times 10^{-29}$
1.3–1.4	1.35	$4.36 \pm 1.10 \times 10^{-29}$	$2.20 \pm 0.55 \times 10^{-29}$	$1.73 \pm 0.49 \times 10^{-29}$
1.4–1.5	1.45	$2.27 \pm 0.59 \times 10^{-29}$	$1.16 \pm 0.30 \times 10^{-29}$	$6.48 \pm 2.15 \times 10^{-30}$
1.5–1.6	1.55	$1.16 \pm 0.29 \times 10^{-29}$	$7.37 \pm 1.80 \times 10^{-30}$	$3.99 \pm 1.06 \times 10^{-30}$
1.6–1.7	1.65	$6.65 \pm 1.66 \times 10^{-30}$	$4.16 \pm 1.03 \times 10^{-30}$	$2.30 \pm 0.64 \times 10^{-30}$
1.7–1.8	1.75	$4.71 \pm 1.19 \times 10^{-30}$	$2.33 \pm 0.59 \times 10^{-30}$	$8.85 \pm 2.86 \times 10^{-31}$
1.8–1.9	1.85	$2.65 \pm 0.69 \times 10^{-30}$	$1.32 \pm 0.34 \times 10^{-30}$	$5.41 \pm 1.93 \times 10^{-31}$
1.9–2.0	1.95	$1.56 \pm 0.38 \times 10^{-30}$	$7.84 \pm 1.89 \times 10^{-31}$	$3.78 \pm 0.94 \times 10^{-31}$
2.0–2.1	2.05	$1.12 \pm 0.27 \times 10^{-30}$	$5.15 \pm 1.25 \times 10^{-31}$	$1.94 \pm 0.50 \times 10^{-31}$
2.1–2.2	2.15	$7.05 \pm 1.71 \times 10^{-31}$	$3.44 \pm 0.84 \times 10^{-31}$	$1.28 \pm 0.34 \times 10^{-31}$
2.2–2.3	2.25	$5.08 \pm 1.24 \times 10^{-31}$	$2.33 \pm 0.57 \times 10^{-31}$	$9.17 \pm 2.49 \times 10^{-32}$
2.3–2.4	2.35	$3.46 \pm 0.84 \times 10^{-31}$	$1.66 \pm 0.40 \times 10^{-31}$	$4.84 \pm 1.27 \times 10^{-32}$
2.4–2.6	2.48	$1.86 \pm 0.45 \times 10^{-31}$	$7.83 \pm 1.90 \times 10^{-32}$	$2.07 \pm 0.55 \times 10^{-32}$
2.6–2.8	2.68	$9.04 \pm 2.20 \times 10^{-32}$	$3.11 \pm 0.77 \times 10^{-32}$	$2.89 \pm 1.18 \times 10^{-33}$
2.8–3.0	2.88	$3.79 \pm 0.94 \times 10^{-32}$	$1.13 \pm 0.29 \times 10^{-32}$	$1.65 \pm 1.23 \times 10^{-33}$
3.0–3.2	3.08	$1.61 \pm 0.39 \times 10^{-32}$	$3.68 \pm 0.92 \times 10^{-33}$	$5.81 \pm 2.38 \times 10^{-34}$
3.2–3.4	3.28	$7.14 \pm 1.72 \times 10^{-33}$	$1.00 \pm 0.25 \times 10^{-33}$	$1.18 \pm 0.58 \times 10^{-34}$
3.4–3.6	3.48	$3.57 \pm 0.87 \times 10^{-33}$	$4.94 \pm 1.26 \times 10^{-34}$	
3.6–3.8	3.68	$1.62 \pm 0.40 \times 10^{-33}$	$1.11 \pm 0.34 \times 10^{-34}$	
3.8–4.0	3.88	$5.99 \pm 1.54 \times 10^{-34}$	$6.78 \pm 2.49 \times 10^{-35}$	
4.0–4.2	4.08	$2.81 \pm 0.78 \times 10^{-34}$		
4.2–4.4	4.28	$6.97 \pm 2.67 \times 10^{-35}$		

Table 3.

Source of systematic error	Error on $E(d^3\sigma/dp^3)$ (%)
1) Uncertainty in the absolute energy scale ($\pm 3\%$)	15
2) Run-to-run systematic variations for different p_T thresholds	15
3) Geometrical acceptance	6
4) Reconstruction efficiency	6
5) Luminosity measurement	6
6) Non-linearity correction (for $p_T > 3$ GeV/c)	5
7) Background subtraction	4
Total	24

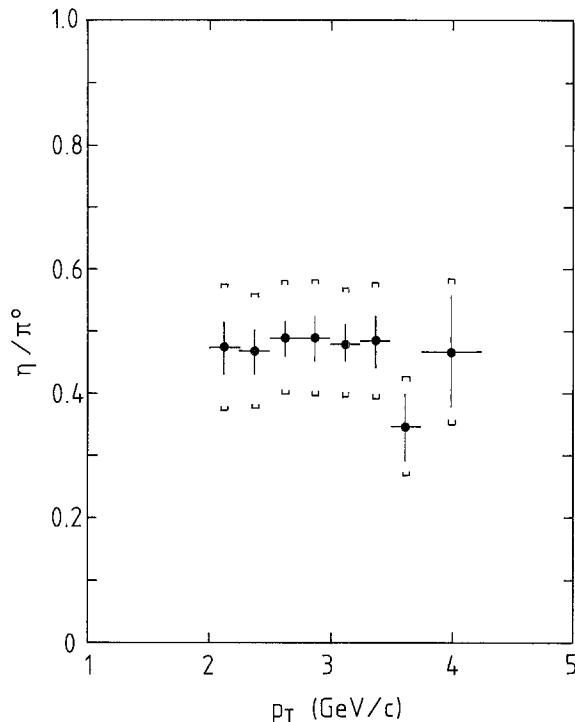


Fig. 6. Corrected η/π^0 ratio versus p_T . Inner error bars are statistical only. Outer error bars include the statistical and systematic errors folded together. The average value over the p_T range $2.0 < p_T < 4.0$ is 0.46 ± 0.02 (statistical) ± 0.06 (systematic)

7. The η/π^0 Ratio

The number of η events was determined by subtracting the background given by the fits in the mass region $450 < m_{\gamma\gamma} < 650$ MeV as a function of p_T in a manner similar to that for the π^0 's. The fits indicate a 2% loss of the true η signal due to the mass cut. This was corrected for in obtaining the true number of observed η events.

Figure 6 shows the η/π^0 ratio corrected for relative geometrical acceptance and reconstruction efficiency as a function of p_T averaged over the ra-

pidity range $2.0 < y < 2.75$. The errors shown are statistical and systematic. The two main sources of systematic error are the background subtraction for the η , and the error on the relative efficiency and acceptance. The former dominates the systematic error for $p_T < 3$ GeV/c, whilst the latter dominates for $p_T > 3$ GeV/c. The ratio shows no apparent p_T dependence over the range $2.0 < p_T < 4.0$ and has an average value of 0.46 ± 0.02 (statistical) ± 0.06 (systematic) over that range. The value given in [4] at $y \sim 0$ is 0.57 ± 0.08 over the p_T range $3 < p_T < 7$ GeV/c, and is independent of \sqrt{s} between 31 and 62 GeV. The result obtained here is essentially equal to the value of $0.45 \pm 0.02 \pm 0.05$ measured at Fermilab [5] at $\sqrt{s} = 13.8$ and 19.4 GeV for $y \sim 0$ and $y \sim 1.3$.

In summary, we have measured the π^0 invariant cross-section in the rapidity range $2.00 < y < 2.75$, and have found that the cross-sections change rapidly with y and have a p_T dependence which is steeper than that observed at $y \sim 0$. We have measured the ratio η/π^0 and found a value which is in agreement with data at other values of rapidity and energy. The knowledge of the π^0 cross-section and η/π^0 ratio in this kinematic region is important for the study of single-photon production, as presented in a separate paper [10].

Acknowledgement. We gratefully acknowledge the CERN EP, EF, and ISR Divisions for their dedicated efforts. We especially appreciate the technical assistance of J. Renaud from the CERN EF Division and G. Mayman from BNL. We thank the collaborating home institutes, the Research Councils, and the US Department of Energy for their support throughout this experiment.

References

1. D. Lloyd Owen et al.: Phys. Rev. Lett. **45**, 89 (1980); D. Lloyd Owen: Single π^0 production cross-sections at $\theta_{em} \sim 90^\circ, 17^\circ$, and 8° at the CERN ISR, Ph.D. dissertation, State University of New York at Stony Brook, November 1979
2. G. Donaldson et al.: Phys. Lett. **73 B**, 375 (1978)
3. C. Kourkoumelis et al.: Z. Phys. C - Particles and Fields **5**, 95 (1980); F.W. Büsser et al.: Phys. Lett. **46 B**, 471 (1973); A.L.S. Angelis et al.: Phys. Lett. **79 B**, 505 (1978)
4. G. Kourkoumelis et al.: Phys. Lett. **84 B**, 277 (1979)
5. G.J. Donaldson et al.: Phys. Rev. Lett. **40**, 684 (1978)
6. H. Gordon et al.: Nucl. Instrum. Methods **196**, 303 (1982); O. Botner et al.: Nucl. Instrum. Methods **196**, 315 (1982); Nucl. Instrum. Methods **179**, 45 (1981); IEEE, Vol. NS-28, 510 (1981)
7. H. Gordon et al.: A hexagonal uranium calorimeter for measuring electromagnetic showers at the CERN ISR. Nucl. Instrum. Methods (submitted for publication)
8. R.L. Ford, W.R. Nelson: SLAC 210 (1978)
9. E. Yen: Phys. Rev. D **10**, 836 (1974)
10. T. Akesson et al.: High- p_T direct photon production at 11° in pp collisions at $\sqrt{s} = 63$ GeV (1983) Phys. Lett. (to be published)